Title

High-Throughput Identification of Loss-of-Function Mutations for Anti-Interferon Activity in the Influenza A Virus NS Segment

Journal

Journal of Virology, 88(17)

ISSN

0022-538X

Authors

Wu, Nicholas C
Young, Arthur P
Al-Mawsawi, Laith Q
et al.

Publication Date

2014-09-01

DOI

10.1128/jvi.01494-14

Peer reviewed

JVI Journals.ASM.org

High-Throughput Identification of Loss-of-Function Mutations for Anti-Interferon Activity in the Influenza A Virus NS Segment

Nicholas C. Wu,[a,b] Arthur P. Young,[a] Laith Q. Al-Mawsawi,[a] C. Anders Olson,[a] Jun Feng,[a] Hangfei Qi,[a] Harding H. Luan,[a] Xinmin Li,[c] Ting-Ting Wu,[a] Ren Sun[a,b,d]

Department of Molecular and Medical Pharmacology, David Geffen School of Medicine, University of California, Los Angeles, California, USA[a]; Molecular Biology Institute, University of California, Los Angeles, California, USA[b]; Department of Pathology and Laboratory Medicine, David Geffen School of Medicine, University of California, Los Angeles, California, USA[c]; AIDS Institute, University of California, Los Angeles, California, USA[d]

ABSTRACT

Viral proteins often display several functions which require multiple assays to dissect their genetic basis. Here, we describe a systematic approach to screen for loss-of-function mutations that confer a fitness disadvantage under a specified growth condition. Our methodology was achieved by genetically monitoring a mutant library under two growth conditions, with and without interferon, by deep sequencing. We employed a molecular tagging technique to distinguish true mutations from sequencing error. This approach enabled us to identify mutations that were negatively selected against, in addition to those that were positively selected for. Using this technique, we identified loss-of-function mutations in the influenza A virus NS segment that were sensitive to type I interferon in a high-throughput fashion. Mechanistic characterization further showed that a single substitution, D92Y, resulted in the inability of NS to inhibit RIG-I ubiquitination. The approach described in this study can be applied under any specified condition for any virus that can be genetically manipulated.

IMPORTANCE

Traditional genetics focuses on a single genotype-phenotype relationship, whereas high-throughput genetics permits phenotypic characterization of numerous mutants in parallel. High-throughput genetics often involves monitoring of a mutant library with deep sequencing. However, deep sequencing suffers from a high error rate (~0.1 to 1%), which is usually higher than the occurrence frequency for individual point mutations within a mutant library. Therefore, only mutations that confer a fitness advantage can be identified with confidence due to an enrichment in the occurrence frequency. In contrast, it is impossible to identify deleterious mutations using most next-generation sequencing techniques. In this study, we have applied a molecular tagging technique to distinguish true mutations from sequencing errors. It enabled us to identify mutations that underwent negative selection, in addition to mutations that experienced positive selection. This study provides a proof of concept by screening for loss-of-function mutations on the influenza A virus NS segment that are involved in its anti-interferon activity.

Type I interferon (IFN) is a major component in the host immune system against influenza A virus infection (1). Briefly, upon influenza virus infection, signal transduction via the mitochondrial antiviral-signaling protein (MAVS) is initiated upon RIG-I ubiquitination (2–4). MAVS signaling leads to phosphorylation of interferon regulatory factor 3 (IRF3) by TANK-binding kinase 1 (TBK1) or IκB kinase-ε (IKKε) (5). Subsequently, it results in the activation of IFN expression (6–8). IFN acts as both a paracrine and an autocrine signaling molecule. Binding of IFN to type I interferon receptors (IFNARs) activates the classical JAK-STAT pathway (9). It then induces the expression of hundreds of interferon-inducible genes (ISGs), which possess varied antiviral functions (1). The IFN antiviral signal can be further amplified by a positive-feedback mechanism (10). Influenza A virus nonstructural protein 1 (NS1), one of the two protein products encoded by segment 8 (NS segment), has acquired multiple strategies to counteract the IFN system (11). It has been reported that NS1 suppresses the IFN system during viral replication in multiple ways, including the inhibition of IRF3 activation (12), the JNK/AP-1 pathway (13), NF-κB signaling (14), PKR (15), and OAS/RNase L (16). To study virus-host interactions, various high-throughput approaches, such as small interfering RNA screening (17–19), yeast two-hybrid screening (20), and mass spectrometry (21), have been employed to identify relevant host genetic elements. However, there is a lack of a high-throughput platform for the viral counterparts of these interactions. Identification of the viral genetic elements involved in the virus-host interaction often requires the construction and analysis of individual mutants. This process has a very low throughput that limits the number of mutants that may be tested. Insertional mutagenesis does permit a higher throughput for identifying critical viral genetic elements and has been applied to hepatitis C virus, Venezuelan equine encephalitis virus, and influenza A virus (22–24). Nonetheless, the resolution of this approach is limited to the protein subdomain level and does not allow the identification of critical residues.

Our previous study has demonstrated the feasibility of using a point mutation library to screen for compensatory mutations at a single-nucleotide resolution (25). Compensatory mutations that conferred a fitness advantage that was increased in relative occur-

Received 23 May 2014 **Accepted** 17 June 2014
Published ahead of print 25 June 2014
Editor: T. S. Dermody
Address correspondence to Ren Sun, RSun@mednet.ucla.edu.

doi:10.1128/JVI.01494-14

rence frequency throughout viral passaging. Consequently, these mutations could be easily identified using 454 pyrosequencing, as previously described (25). Although this previous approach can rapidly identify gain-of-function mutations that provide fitness benefits, the method lacks the power to distinguish between neutral and deleterious mutations. The majority of point mutations in a mutant library exhibit an occurrence frequency of <0.1%, which is lower than the error rate of next-generation sequencing (~0.1 to 1%). True mutations cannot be distinguished from sequencing errors unless there is positive enrichment. As a result, any loss-of-function mutations that confer a fitness disadvantage cannot be identified. For example, a mutation that has a 10-fold decrease in occurrence frequency during passaging (0.01% to 0.001%) would be interpreted to confer a neutral phenotype (~0.1% to ~0.1%) in the next-generation sequencing data due to the sequencing error rate. This limitation poses a unique challenge in utilizing next-generation sequencing technology to screen for loss-of-function mutations that carry a fitness defect in large mutant pools. However, loss-of-function mutations often provide valuable information that may be used to characterize the genetic elements involved in the virus-host interaction. It is therefore important to establish a platform to identify loss-of-function mutations that undergo negative selection in a high-throughput manner.

In this study, we describe an approach that incorporates a sensitive deep sequencing technique to systematically identify loss-of-function mutations. It allows the identification of mutations that are negatively selected against, in addition to those that are positively selected for. We provide a proof of concept of our approach by identifying residues in the influenza virus NS segment that are critical for anti-IFN function. This is achieved by monitoring a point mutation library of the NS segment under two growth conditions: with and without IFN treatment. By utilizing a tag-based sequencing strategy, we were able to distinguish true mutations from sequencing error. The relative interferon sensitivities for 1,021 NS missense mutations were then estimated by comparing the mutant profiles between the two conditions. Experimental validation led to the identification of a novel interferon-sensitive substitution, NS1 D92Y. Further characterization suggests that NS1 D92Y has a defect in blocking RIG-I ubiquitination, which is a critical step in the interferon signaling pathway. To our knowledge, this is the first example of the systematic identification of loss-of-function mutations involved in the virus-host interaction. This approach can potentially be adapted to any specified condition for any virus that can be genetically manipulated.

MATERIALS AND METHODS

Viral mutant library and point mutations. The NS segment point mutation library was constructed as previously described (25) using the eight-plasmid reverse genetic system of influenza virus A/WSN/1933 (H1N1) (26). Briefly, the NS segment was PCR amplified using the error-prone polymerase Mutazyme II (Stratagene, La Jolla, CA) and cloned into BsmBI-digested parental vector pHW2000. Ligations were carried out with a high concentration of T4 ligase (Life Technologies, Carlsbad, CA). Transformations were carried out with electrocompetent MegaX DH10B T1R cells (Life Technologies). Sequencing of individual clones showed that the clones in the plasmid mutant library had an average of one to two point mutations per clone. The plasmid mutant library was purified from a collection of >200,000 clones using a Qiagen plasmid maxikit (Qiagen Sciences, Germantown, MD). Point mutations for experimental validation were constructed using a QuikChange XL mutagenesis kit (Stratagene) according to the manufacturer's instructions.

Transfections, infections, and determination of viral titers. Cells of the C227 cell line, a dominant negative cell line stably expressing IRF3 derived from human embryonic kidney 293T (HEK293T) cells (27), were transfected with the NS mutant library plasmid (for screening) or NS point mutation plasmid (for validation) plus seven other wild-type (WT) plasmids using Lipofectamine 2000 (Life Technologies). Supernatant was replaced with fresh cell growth medium at 24 h and 48 h posttransfection. At 72 h posttransfection, supernatant containing infectious virus was harvested, filtered through a 0.45-μm-pore-size mixed cellulose ester (MCE) filter, and stored at −80°C. The 50% tissue culture infective dose was measured on A549 cells (human lung carcinoma cells). Virus from C227 cell transfection was used to infect A549 cells at a multiplicity of infection (MOI) of 0.05. Infected cells were washed three times with phosphate-buffered saline, followed by the addition of fresh cell growth medium at 2 h postinfection. Virus was harvested at 24 h postinfection. For infection under IFN treatment, 30 U/ml of alpha IFN (IFN-α; Fitzgerald, Acton, MA) was added at 18 h preinfection and the concentration was maintained throughout the course of infection. The viruses in the mutant library were passaged for two rounds in A549 cells before they were subjected to deep sequencing. Due to the huge complexity of the mutant library, >35 million cells were used at both viral rescue and passaging to avoid any bottleneck effect.

Sequencing library preparation. The viral RNA was extracted using a QIAamp viral RNA kit (Qiagen Sciences) and reverse transcribed to cDNA using SuperScript III reverse transcriptase (Life Technologies). A two-step PCR was performed for sequencing library preparation. In the first PCR, the NS segment was divided into six amplicons generated using the following primers: for amplicon 1, primers 5′-CTA CAC GAC GCT CTT CCG ATC TNN NNN NTA ATG GAT CCA AAC ACT GTG T-3′ and 5′-TGC TGA ACC GCT CTT CCG ATC TNN NNN NCC AGC ACG GGT GGC TGT-3′; for amplicon 2, primers 5′-CTA CAC GAC GCT CTT CCG ATC TNN NNN NTC TTG GTC TGG ACA TCG AA-3′ and 5′-TGC TGA ACC GCT CTT CCG ATC TNN NNN NTT TCT GCT TGG GCA TGA GC-3′; for amplicon 3, primers 5′-CTA CAC GAC GCT CTT CCG ATC TNN NNN NAT GTC AAG GCA CTG GTT CAT-3′ and 5′-TGC TGA ACC GCT CTT CCG ATC TNN NNN NCG CCA ACA ATT GTC CCC T-3′; for amplicon 4, primers 5′-CTA CAC GAC GCT CTT CCG ATC TNN NNN NTA AGG GCC TTC ACC GAA G-3′ and 5′-TGC TGA ACC GCT CTT CCG ATC TNN NNN NTC ATT ACT GCT TCT CCA AGC-3′; for amplicon 5, primers 5′-CTA CAC GAC GCT CTT CCG ATC TNN NNN NAA CAC AGT TCG AGT CTC TGA-3′ and 5′-TGC TGA ACC GCT CTT CCG ATC TNN NNN NCT ATT CTC TGT TAT CTT CAG TC-3′; and for amplicon 6, primers 5′-CTA CAC GAC GCT CTT CCG ATC TNN NNN NTG GCG GGA ACA ATT AGG TC-3′ and 5′-TGC TGA ACC GCT CTT CCG ATC TNN NNN NAT AAG CTG AAA CGA GAA AGT T-3′.

The six amplicon products were then mixed at an equal molar ratio and subjected to the second PCR, which generated multiple copies of each tagged template, using the primers 5′-AAT GAT ACG GCG ACC ACC GAG ATC TAC ACT CTT TCC CTA CAC GAC GCT CTT CCG-3′ and 5′-CAA GCA GAA GAC GGC ATA CGA GAT CGG TCT CGG CAT TCC TGC TGA ACC GCT CTT CCG-3′. For the individual sample population, ~1 million copies of mixed amplicon products were provided as input for the second PCR. The product from the second PCR was then deep sequenced using an Illumina HiSeq 2000 sequencer.

Data analysis. Sequencing reads were mapped by use of the Burrows-Wheeler alignment tool (BWA) with a maximum of six mismatches and no gap (28). Amplicons with the same tag were grouped into a read cluster and further conflated into an error-free read, as described in reference 29. True mutations were called only if the mutation occurred in >90% of the reads within a read cluster. Read clusters with less than three reads were removed. All analyses were performed with custom Python scripts that are available upon request. The IFN sensitivity for each point mutation was

TABLE 1 Basic information for the six amplicons

Amplicon	Location[a] (nt)	Coverage[b] (no. of reads)	
		Without IFN	With IFN
1	33–178	235,410	207,758
2	179–324	189,658	182,160
3	325–470	255,201	216,035
4	471–616	258,799	214,646
5	601–741	238,791	205,080
6	695–826	210,066	218,157

[a] The first nucleotide after the forward primer to the last nucleotide before the reverse primer.
[b] Coverage of error-free reads.

computed by use of the occurrence frequency without IFN/occurrence frequency with IFN. Coverage information for individual amplicons is shown in Table 1.

Real-time reverse transcription-qPCR. Supernatant from infected cells was processed with a QIAamp viral RNA kit (Qiagen Sciences). Viral RNA was reverse transcribed with SuperScript III reverse transcriptase (Invitrogen) using random hexamers. Quantitative PCR (qPCR) was performed on a DNA Engine Opticon 2 system (Bio-Rad, Irvine, CA) using SYBR green (Life Technologies) with primers 5′-GAC GAT GCA ACG GCT GGT CTG-3′ and 5′-ACC ATT GTT CCA AC TCC TTT-3′.

Immunoprecipitation and immunoblotting. HEK293T cells seeded on a 6-well plate were transfected using Lipofectamine 2000 (Life Technologies). At 24 h posttransfection, cells were infected with Sendai virus (SeV; 100 U/ml). At 18 h postinfection, cells were lysed with lysis buffer (50 mM Tris, pH 7.5, 150 mM NaCl, 1.0% Nonidet P-40, 10% glycerol, 10 g/ml aprotinin, 10 g/ml pepstatin, 0.5 mM phenylmethylsulfonyl fluoride). Lysates were incubated with an EZview red anti-Flag M2 affinity gel (Sigma, St. Louis, MO) for 6 h. Beads were washed 3 times with lysis buffer. Proteins were eluted with SDS loading buffer (50 mM Tris-HCl, pH 6.8, 2% SDS, 10% glycerol, 1% β-mercaptoethanol, 12.5 mM EDTA, 0.02% bromophenol blue) and heated at 90°C for 5 min. Mouse anti-Flag antibody (Sigma), mouse anti-β-actin antibody (Sigma), mouse anti-hemagglutinin (anti-HA) antibody (Sigma), rabbit anti-NS1 antibody (GeneTex, Irvine, CA), sheep horseradish peroxidase-conjugated anti-mouse immunoglobulin G (GE Healthcare, Pasadena, CA), and donkey horseradish peroxidase-conjugated anti-rabbit immunoglobulin G (GE Healthcare) were used for protein detection.

Protein stability. HEK293T cells were transfected with Flag-tagged NS1. At 24 h posttransfection, 40 μg/ml cycloheximide was added. Transfected cells were harvested at the time points indicated below. The relative amount of cellular Flag-tagged NS1 was quantified by densitometry.

Luciferase assay. HEK293T cells seeded on 48-well plates were transfected with 50 ng of firefly luciferase reporter plasmid, 5 ng of PGK renilla luciferase, and other indicated expression plasmids using Lipofectamine 2000 (Life Technologies). SeV (100 U/ml) was added at 24 h posttransfection, and a luciferase activity assay was performed at 48 h posttransfection using a Promega dual-luciferase assay kit according to the manufacturer's instructions (Promega, Madison, WI). For the assay of overexpression-mediated promoter activity, a luciferase activity assay was performed at 24 h posttransfection. Adjusted luciferase activity was calculated by normalizing the firefly luciferase activity to the activity of the internal renilla luciferase controls. Fold induction was calculated by dividing the adjusted luciferase activities in the treated samples by those in the untreated samples.

RESULTS

Experimental design of high-throughput screening. The underlying rationale of the high-throughput screening for loss-of-function mutations is that by replacing a residue phenotypically critical under one particular growth condition, the virus would display a fitness deviation compared to that in the control environment (Fig. 1A). We propose that a mutant library can be employed to identify such substitutions. The fitness deviation caused by a particular substitution would be reflected by the difference of its occurrence frequency between two conditions. This establishes the conceptual foundation for the systematic identification of loss-of-function mutations that are selected against under a specified growth condition but not under the control growth condition.

In this study, we aimed to provide a proof of concept by identifying interferon-sensitive mutations on the influenza A virus NS segment. We constructed a plasmid mutant library of the NS segment of influenza virus A/WSN/1933 using error-prone PCR. A mutation rate of one to two point mutations was achieved to minimize any genetic interactions that could potentially confound the results. As a result, on average, each point mutation had an occurrence frequency of ~0.04 to 0.08% in the mutant library. This mutation rate was significantly higher than the natural mutation rate of influenza virus, which has been shown to be on the order of 10^{-6} mutation per site per infectious cycle (30), but was lower than the sequencing error rate in next-generation sequencing (~0.1 to 1%). The plasmid mutant library consisted of a collection of >200,000 clones, allowing sufficient coverage of individual point mutations. The viral mutant library was rescued in

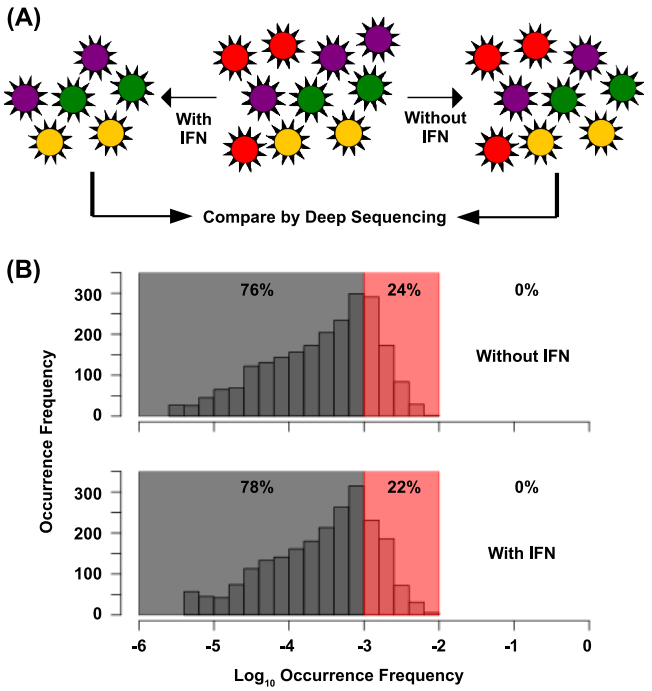

FIG 1 Single-nucleotide-resolution interferon sensitivity profiling of the NS segment. (A) The viral mutant library (middle) was passaged under two different growth conditions: with and without IFN. Each circle represents an individual viral particle. Different colors represent mutants with different genotypes. In this depiction, the red virus genotype represents a mutant with a defect in anti-IFN function. Here, the red virus has a normal replication phenotype without IFN (right) but a deleterious phenotype in the presence of IFN (left). (B) Histograms show the distribution of the occurrence frequency of individual point mutations within the mutant library after passage with and without IFN. The sequencing error rate margin (0.1 to 1%) is shaded in red. Frequencies below the sequencing error rate (<0.1%) are shaded in gray. The percentages of point mutations within the different ranges of occurrence frequency are also shown.

HEK293T cells using the eight-plasmid system, as described previously (26), and then passaged under two different growth conditions, with or without IFN. The viral mutant library was passaged for two 24-h rounds in A549 cells. Consequently, two viral populations (passaged with or without IFN) derived from the same library were deep sequenced to quantify the occurrence frequency of individual point mutations. During each step in both viral rescue and passaging, >35 million cells were employed to avoid any bottleneck effect that would randomly drift the occurrence frequency of each point mutation in the mutant pool. In addition, a low MOI (MOI = 0.05) was used to minimize transcomplementation. As a result, the relative fitness of each point mutation would be reflected from its occurrence frequency.

Next-generation sequencing error poses a unique challenge to identify loss-of-function mutations that confer a fitness disadvantage. The majority of point mutations in our mutant library have an occurrence frequency below the Illumina sequencing error rate (~0.1 to 1%). During selection, a given point mutation can be enriched, remain unchanged, or diminished in occurrence frequency, depending on its relative fitness under the specified growth condition. However, only mutations that are significantly enriched would be identified by conventional deep sequencing techniques due to the high sequencing error rate. Deleterious or phenotypically neutral mutations, which have a low occurrence in the population, are not distinguishable from each other. Here, a nucleotide tagging strategy was adapted to distinguish true mutations from sequencing errors (29). Briefly, a two-step PCR approach to sequencing error correction was employed in the preparation of the DNA sequencing library. The first PCR assigned a 12-N nucleotide tag to individual molecules. Six amplicons, each with ~140 bp, were generated in the first PCR to cover the NS segment (from nucleotides 33 to 826) (Table 1). The input amount for the second PCR was well controlled, such that each tagged template would be sequenced ~10 times. The complexity of the tag population (4^{12}, or ≈17 million) was >100-fold higher than the number of tagged templates being sequenced (~0.16 million per amplicon). Therefore, sequencing reads generated from the same template would share a unique tag. True mutations can be distinguished from sequencing errors by clustering reads that share the same tag (read cluster). True mutations appear in all reads within a read cluster. In contrast, sequencing errors appear in only a small fraction of the reads within a read cluster. Ultimately, an error-free read will be generated from each read cluster. This approach allowed us to identify loss-of-function mutations that decreased in frequency during viral passage without being obscured by sequencing errors.

Interferon sensitivity profiling result. Each read cluster had an average size of ~10 reads in the deep sequencing data. True mutations were called only if the mutation occurred in >90% of the reads within a read cluster. Furthermore, read clusters with <3 reads were removed to increase the level of confidence in distinguishing true mutations from sequencing errors. An even coverage across the NS segment ranging from ~180,000 to ~260,000 error-free reads was obtained (Table 1). This coverage enabled mutations with an occurrence frequency on the order of 10^{-5} to be detected.

As expected, none of the point mutations in the passaged mutant library had an occurrence frequency above the sequencing error margin (>1%), whereas 22 to 24% had occurrence frequencies that fell within the sequencing error margin (0.1 to 1%) and 76 to 78% had occurrence frequencies that were below the sequencing error margin (<0.1%) (Fig. 1B). This occurrence frequency distribution showed that none of the point mutations conferred a significant replication fitness advantage. It also suggested that the occurrence frequency of all point mutations within the mutant pool would not be accurately estimated if the sequencing error were not corrected. It fully confirmed the necessity to distinguish true mutations from sequencing error using the molecular tag approach. This strategy increased the sensitivity of next-generation sequencing, such that the occurrence frequency of individual mutations within the mutant library could be accurately determined.

The occurrence frequency of individual mutations exhibited a Pearson correlation of 0.91 between the two passaging conditions. This indicated that most mutations on the NS segment do not exhibit a relative fitness deviation dependent on IFN. The IFN sensitivities of individual mutations can be computed by the ratio of their occurrence frequency between the two conditions: IFN sensitivity = occurrence frequency without IFN/occurrence frequency with IFN.

We aimed to identify loss-of-function mutations that disrupt the anti-IFN function. These loss-of-function mutations would be negatively selected against under IFN treatment but not under the control growth condition. Therefore, they would exhibit a higher relative fitness cost (lower occurrence frequency) in the presence of IFN than under the control growth condition. Consequently, loss-of-function mutations would be associated with a high IFN sensitivity. Our data analysis included only mutations that were sufficiently abundant under the control condition, which allowed the IFN sensitivity to be computed with a higher statistical confidence. A cutoff was set at >0.02%, which was reached by ~60% of all possible point mutations. Only mutations that satisfied the confidence cutoff were included in our analysis, unless otherwise stated.

Although NS1 is important for counteracting the antiviral effects of IFN, it is nonessential for viral replication (31). As a result, defective NS1 would confer a higher IFN sensitivity than its functionally intact counterpart. It is expected that the mean IFN sensitivity would be the lowest for silent mutations, followed by missense mutations, and would be the greatest for nonsense mutations. Indeed, the IFN sensitivities of nonsense mutations (mean IFN sensitivity = 1.53) were significantly greater than those of missense mutations (mean IFN sensitivity = 1.13) ($P = 2e^{-6}$, Wilcoxon rank sum test), whereas the IFN sensitivities of missense mutations were significantly greater than those of silent mutations (mean IFN sensitivity = 0.97) ($P = 1e^{-9}$, Wilcoxon rank sum test). These results support the validity of the data.

IFN sensitivity was computed for each of the 1,021 missense mutations that satisfied the confidence cutoff (Fig. 2). A total of 21 missense mutations displayed an IFN sensitivity greater than 3 standard deviations above the mean (IFN sensitivity >2.46). Included in this set of IFN-sensitive mutations was an arginine (R)-to-leucine (L) substitution at NS1 residue 38. R38 has been reported to be absolutely required for NS1 RNA-binding activity (32, 33), which facilitates the masking of viral RNA to inhibit IFN activation during viral infection (12–14). In fact, the mean IFN sensitivity for all missense mutations at residues critical for RNA-binding activity, P31, D34, R35, R38, K41, G45, R46, and T49 (mean IFN sensitivity = 1.32), was significantly greater than that for all missense mutations throughout the NS segment ($P = 5e^{-4}$,

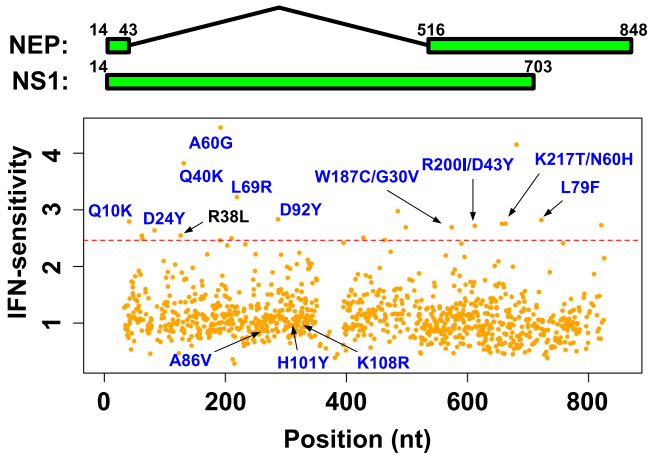

FIG 2 IFN sensitivity profiling. (Top) The coding regions of NS1 and NEP are depicted as green rectangles. (Bottom) The IFN sensitivity for individual missense mutations is plotted versus the nucleotide (nt) positions. Only mutations with an occurrence frequency of >0.02% under the control condition are shown. Red dotted line, 3 standard deviations above the mean. Labels indicate the corresponding amino acid substitution. Substitutions in NEP are indicated after a slash (/). Substitutions in blue represent the mutations that were individually constructed and analyzed in this study. Substitutions in black are at residues with known biological functions.

Wilcoxon rank sum test). This result confirms the reliability of our data set.

Validation of individual interferon-sensitive mutations identified from the screen. Next, we aimed to identify novel loss-of-function mutations that disrupt the anti-IFN function of NS1. We randomly selected 9 of the 21 missense mutations in the NS segment that had an IFN sensitivity greater than 3 standard deviation above the mean (Fig. 3). Individual mutants were constructed and analyzed. The viral copy numbers were compared using qPCR at 24 h after replication in A549 cells (MOI = 0.05) with (30 U/ml) and without IFN-α. Six of the nine mutants displayed a >2-fold higher IFN sensitivity than the WT in this assay. Three of the six missense mutations resulted in substitutions in the NS1 RNA-binding domain (D24Y, Q40K, and A60G) and one substitution each in the NS1 effector domain (D92Y), the nuclear export protein (NEP) (L79F), and the overlapping reading frame of the NS1 effect domain (W187C) with NEP (G30V). As a control, three missense mutations on NS1 (A86V, H101Y, and K108R) that had an IFN sensitivity ranging from 0.85 to 0.98 in the profiling data were included in this validation assay. None of them displayed any phenotypic difference from the WT in this assay. The validation result verifies the design of our high-throughput screening approach. The NS1 D92Y mutant showed the strongest IFN sensitivity phenotype (12-fold higher than that of the WT, $P = 10^{-5}$) among the validated mutants and was selected for further characterization.

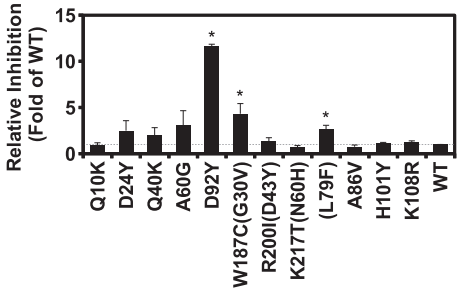

FIG 3 Identification of novel IFN-sensitive mutations. The relative viral replication inhibition by IFN-α was measured by determination of the RNA copy number using qPCR. Error bars represent the standard errors of the means (SEMs) from three independent experiments. Gray dotted line, WT level. Substitutions in NEP are shown in parentheses. Mutants for which the *P* value was <0.05 are indicated with asterisks. A one-tailed *t* test was performed to compute the *P* value.

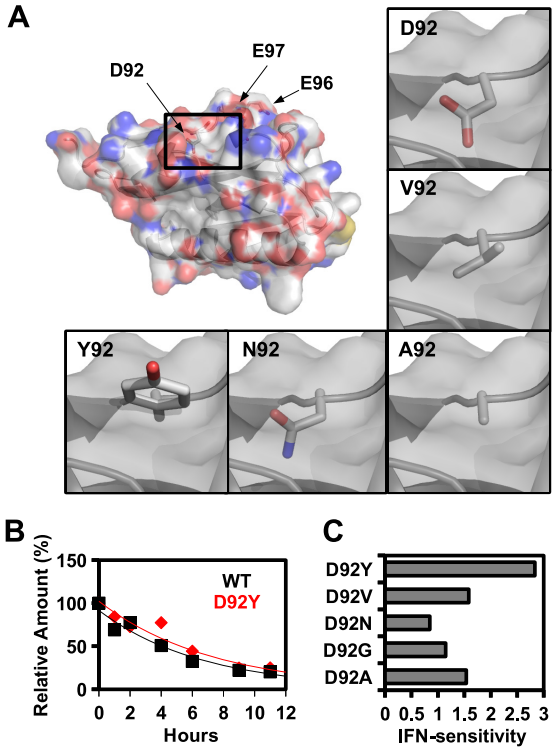

FIG 4 Structural and stability effects of substitutions at NS1 residue 92. (A) The structures for different substitutions at residue 92 are displayed. The rotamers for different substitutions were generated by free energy minimization simulation using Rosetta software (36). Only the D92Y substitution reduced the pocket space. An NS1 monomer (chain A of the structure with PDB accession number 2GX9) was employed (50). (B) Transiently transfected HEK293T cells were treated with 40 μg/ml cycloheximide. The NS1 protein level at different time points was quantified by densitometry to examine the rate of protein degradation. (C) IFN sensitivities for the profiled missense substitutions at D92 are shown.

Mechanistic characterization of the D92Y mutation reveals its role in the IFN signaling pathway. Residue 92 on NS1 has been reported to be a tumor necrosis factor alpha (TNF-α) resistance determinant (34). Human influenza viruses carry a conserved aspartic acid at this position, whereas avian influenza viruses carry a glutamic acid. The D92E substitution in NS1 has been shown to contribute to TNF-α resistance, while it exerts no effect on IFN sensitivity in human influenza virus (34, 35). On the other hand, our data suggest that replacement of residue 92 with tyrosine significantly increases IFN sensitivity (Fig. 3). We first performed a structural analysis of this mutant using Rosetta software and the parameters from row 16 of Table 1 in the article by Kellogg et al. (36). The energy minimization simulation predicts that D92Y disrupted a hydrophobic pocket on NS1 due to the volume increase from aspartic acid to tyrosine (Fig. 4A). We then performed a

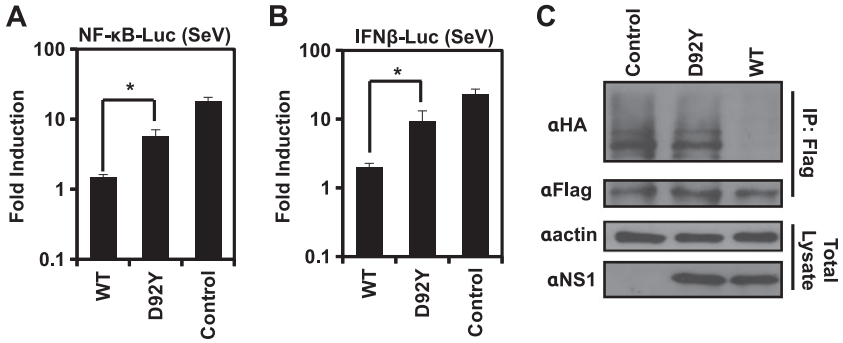

FIG 5 Characterization of the NS1 D92Y substitution. (A) SeV-mediated NK-κB promoter activities were measured by luciferase assay. (B) SeV-mediated IFN-β promoter activities were measured by luciferase assay. (A and B) Mean values are plotted. Error bars represent the standard error of the mean (SEM) from three independent experiments. All differences between D92Y and WT were significant ($P < 0.05$), as indicated with asterisks. A two-tailed *t* test was performed to compute the *P* value. (C) SeV-mediated ubiquitination of RIG-I was measured by immunoprecipitation (IP) and Western blotting.

cycloheximide blocking experiment to examine the protein stability effect of D92Y on NS1. The rates of degradation of D92Y NS1 and WT NS1 did not display a significant difference (Fig. 4B), suggesting that D92Y did not affect NS1 protein stability. As a result, residue 92 may be involved in maintaining the conformation of the hydrophobic pocket critical for the anti-IFN function. Furthermore, our sequencing data also showed that D92V, D92N, D92G, and D92A had no effect (Fig. 4C). Structural modeling demonstrated that these substitutions did not significantly alter the conformation of the hydrophobic pocket (Fig. 4A). These results are consistent with the importance of maintaining the hydrophobic pocket for counteracting the antiviral effects of IFN.

The NS1 effector domain has been shown to mediate the inhibition of RIG-I ubiquitination (37) and hence the inhibition of IFN expression and potentially the positive-feedback mechanism (3, 4, 38). We hypothesized that D92Y abolished the suppression of RIG-I ubiquitination. We first looked at the downstream effectors of RIG-I ubiquitination, NF-κB and IFN-β (2, 3, 38), using a luciferase reporter assay. Indeed, compared to the WT, the D92Y mutant lost the ability to suppress NF-κB promoter activation (Fig. 5A) and IFN-β promoter activation (Fig. 5B) induced by Sendai virus (SeV). These results are consistent with our hypothesis that the suppression of RIG-I ubiquitination can be abolished by the D92Y mutation. Consequently, we performed a coimmunoprecipitation assay to test the effect of D92Y on the inhibition of SeV-induced RIG-I ubiquitination (Fig. 5C). HA-tagged ubiquitin and Flag-tagged RIG-I were cotransfected in the presence of the NS1 WT or D92Y mutant. Flag-tagged RIG-I was immunoprecipitated 18 h after SeV infection. Ubiquitination of RIG-I was then detected by HA antibody. Indeed, ubiquitination of RIG-I was inhibited by the NS1 WT but not the NS1 D92Y mutant. Taken together, our results indicate that residue 92 is critical for the inhibition of RIG-I ubiquitination, an important step for IFN signaling (3), likely by maintaining the conformation of the hydrophobic pocket.

DISCUSSION

Identification of loss-of-function viral mutations is critical for understanding virus-host interactions. They often represent mechanisms essential for viral replication under a specified growth condition. Mechanistic interrogation of the identified mutations offers further insight into their structure-function. The impact can be translated to vaccine and antiviral drug development. For example, temperature-sensitive mutations and anti-interferon actions provide the foundation for influenza virus vaccine development (39, 40). In addition, the cell entry mechanism of influenza virus has been suggested to be a potent antiviral target (41–43). This and many other examples highlight the medical importance of characterization of viral genetic elements. However, there is a lack of a high-throughput platform to screen for these functional elements.

In vitro culture systems and reverse genetics offer powerful tools to study virus-host interactions in laboratory settings. They are well established for several medically important viruses, such as hepatitis C virus (44–46), HIV (47), and influenza virus (26, 48). Functional characterization of viral genetic elements often relies on constructing and analyzing individual mutants with multiple assays. The low throughput of this process limits the number of mutants to be analyzed. In this study, we overcame this challenge by coupling saturation mutagenesis with a sensitive deep sequencing technique. This allowed us to monitor negative selection in addition to positive selection. The functionality of each mutation was inferred by comparing the mutational profile of a point mutation library under different growth conditions. This approach is rapid, unbiased, and comprehensive. We provided a proof of concept for this differential profiling technique by identifying IFN-sensitive mutations in the influenza A virus NS segment.

To our knowledge, this is the first example of the utilization of a high-throughput genetic platform at a single-nucleotide resolution to identify loss-of-function mutations under a specific growth condition. Our previous study described a similar technique, which utilized deep sequencing to monitor a mutant library to identify compensatory mutations (25). However, the approach described in our previous study was capable of identifying only mutations that were enriched during selection. This is because without significant enrichment during viral passaging, the occurrence frequencies of most, if not all, point mutations would remain below the sequencing error rate. The phenotypic effects of nonenriched point mutations could not be inferred, as it was impossible to partition them from sequencing errors. In this study, an error correction technique was implemented to distinguish true mutations from sequencing errors. This critical step allowed the monitoring of individual point mutations even if their occur-

rence frequency was below the sequencing error rate. Therefore, we are now capable of identifying loss-of-function mutations that decrease in frequency during IFN treatment.

We anticipate that the power of the screening technique described in this study will increase as sequencing technology advances. Increasing sequencing depth will minimize the sampling error of individual point mutations and, hence, increase the accuracy in computing the occurrence frequency of individual point mutations and improve the precision of estimating their deviations in fitness between different growth conditions. Additionally, a longer read length will enable the examination of different mutations existing in the same clone, which will allow the study of genetic interactions among point mutations.

A recent study has suggested that besides the NS segment, other segments of influenza A virus also possess the ability to counteract IFN activity (49). Although we applied the screening technique only to the NS segment, it will be worthwhile to extend the analysis to the whole genome or other viral genetic backgrounds in the future. Moreover, this approach is not limited to interferon. It can also be employed to identify temperature-sensitive mutations as well as viral genetic elements involved in the virus-host interaction under a specific cellular or immune response, such as the response to apoptosis, autophagy, endoplasmic reticulum stress, NK cells, and macrophages. In summary, the genetic approach presented in this study has a wide range of potential applications to identify residues involved in virus-host interactions. More importantly, our methodology can be applied to probe any virus that can be genetically manipulated in the laboratory.

ACKNOWLEDGMENTS

We thank G. Hobom and Y. Liang for the eight-plasmid reverse genetics system for the A/WSN/1933 virus and J. Zhou and J. Yoshizawa for performing the high-throughput sequencing experiment.

This work was supported by the National Institutes of Health (reference R21-AI-110261), a UCLA Molecular Biology Whitcome predoctoral fellowship, Oppenheimer Endowment Awards and Clinical Translational Seed Grants, and the UCLA Jonsson Comprehensive Cancer Center.

N.C.W. and R.S. designed the experiment, A.P.Y. created the plasmid library, N.C.W. conducted the experiments, X.L. performed the sequencing, N.C.W. performed the sequencing mapping and data analysis, L.Q.A.-M., J.F., and H.H.L. provided experimental support, C.A.O., H.Q., and T.-T.W. provided important intellectual input, N.C.W. and R.S. supervised the project, and N.C.W. and R.S. wrote the text.

REFERENCES

1. **Randall RE, Goodbourn S.** 2008. Interferons and viruses: an interplay between induction, signalling, antiviral responses and virus countermeasures. J. Gen. Virol. **89:**1–47. http://dx.doi.org/10.1099/vir.0.83391-0.
2. **Rehwinkel J, Tan CP, Goubau D, Schulz O, Pichlmair A, Bier K, Robb N, Vreede F, Barclay W, Fodor E, Reis e Sousa C.** 2010. RIG-I detects viral genomic RNA during negative-strand RNA virus infection. Cell **140:**397–408. http://dx.doi.org/10.1016/j.cell.2010.01.020.
3. **Gack MU, Shin YC, Joo C-H, Urano T, Liang C, Sun L, Takeuchi O, Akira S, Chen Z, Inoue S, Jung JU.** 2007. Trim25 ring-finger E3 ubiquitin ligase is essential for RIG-I-mediated antiviral activity. Nature **446:**916–920. http://dx.doi.org/10.1038/nature05732.
4. **Yoneyama M, Fujita T.** 2009. RNA recognition and signal transduction by RIG-I-like receptors. Immunol. Rev. **227:**54–65. http://dx.doi.org/10.1111/j.1600-065X.2008.00727.x.
5. **Fitzgerald KA, McWhirter SM, Faia KL, Rowe DC, Latz E, Golenbock DT, Coyle AJ, Liao S-M, Maniatis T.** 2003. IKKepsilon and TBK1 are essential components of the IRF3 signaling pathway. Nat. Immunol. **4:**491–496. http://dx.doi.org/10.1038/ni921.
6. **Yoneyama M, Suhara W, Fujita T.** 2002. Control of IRF-3 activation by phosphorylation. J. Interferon Cytokine Res. **22:**73–76. http://dx.doi.org/10.1089/107999002753452674.
7. **Hou F, Sun L, Zheng H, Skaug B, Jiang Q-X, Chen ZJ.** 2011. MAVS forms functional prion-like aggregates to activate and propagate antiviral innate immune response. Cell **146:**448–461. http://dx.doi.org/10.1016/j.cell.2011.06.041.
8. **Hiscott J, Pitha P, Genin P, Nguyen H, Heylbroeck C, Mamane Y, Algarte M, Lin R.** 1999. Triggering the interferon response: the role of IRF-3 transcription factor. J. Interferon Cytokine Res. **19:**1–13. http://dx.doi.org/10.1089/107999099314360.
9. **Platanias LC.** 2005. Mechanisms of type-I- and type-II-interferon-mediated signalling. Nat. Rev. Immunol. **5:**375–386. http://dx.doi.org/10.1038/nri1604.
10. **Taniguchi T, Takaoka A.** 2001. A weak signal for strong responses: interferon-alpha/beta revisited. Nat. Rev. Mol. Cell Biol. **2:**378–386. http://dx.doi.org/10.1038/35073080.
11. **Hale BG, Randall RE, Ortn J, Jackson D.** 2008. The multifunctional NS1 protein of influenza A viruses. J. Gen. Virol. **89:**2359–2376. http://dx.doi.org/10.1099/vir.0.2008/004606-0.
12. **Talon J, Horvath CM, Polley R, Basler CF, Muster T, Palese P, García-Sastre A.** 2000. Activation of interferon regulatory factor 3 is inhibited by the influenza A virus NS1 protein. J. Virol. **74:**7989–7996. http://dx.doi.org/10.1128/JVI.74.17.7989-7996.2000.
13. **Ludwig S, Wang X, Ehrhardt C, Zheng H, Donelan N, Planz O, Pleschka S, García-Sastre A, Heins G, Wolff T.** 2002. The influenza A virus NS1 protein inhibits activation of Jun N-terminal kinase and AP-1 transcription factors. J. Virol. **76:**11166–11171. http://dx.doi.org/10.1128/JVI.76.21.11166-11171.2002.
14. **Wang X, Li M, Zheng H, Muster T, Palese P, Beg AA, García-Sastre A.** 2000. Influenza A virus NS1 protein prevents activation of NF-kappaB and induction of alpha/beta interferon. J. Virol. **74:**11566–11573. http://dx.doi.org/10.1128/JVI.74.24.11566-11573.2000.
15. **Bergmann M, Garcia-Sastre A, Carnero E, Pehamberger H, Wolff K, Palese P, Muster T.** 2000. Influenza virus NS1 protein counteracts PKR-mediated inhibition of replication. J. Virol. **74:**6203–6206. http://dx.doi.org/10.1128/JVI.74.13.6203-6206.2000.
16. **Min J-Y, Krug RM.** 2006. The primary function of RNA binding by the influenza A virus NS1 protein in infected cells: inhibiting the 2′-5′ oligo (A) synthetase/RNase L pathway. Proc. Natl. Acad. Sci. U. S. A. **103:**7100–7105. http://dx.doi.org/10.1073/pnas.0602184103.
17. **Panda D, Das A, Dinh PX, Subramaniam S, Nayak D, Barrows NJ, Pearson JL, Thompson J, Kelly DL, Ladunga I, Pattnaik AK.** 2011. RNAi screening reveals requirement for host cell secretory pathway in infection by diverse families of negative-strand RNA viruses. Proc. Natl. Acad. Sci. U. S. A. **108:**19036–19041. http://dx.doi.org/10.1073/pnas.1113643108.
18. **König R, Stertz S, Zhou Y, Inoue A, Hoffmann H-H, Bhattacharyya S, Alamares JG, Tscherne DM, Ortigoza MB, Liang Y, Gao Q, Andrews SE, Bandyopadhyay S, Jesus PD, Tu BP, Pache L, Shih C, Orth A, Bonamy G, Miraglia L, Ideker T, García-Sastre A, Young JAT, Palese P, Shaw ML, Chanda SK.** 2010. Human host factors required for influenza virus replication. Nature **463:**813–817. http://dx.doi.org/10.1038/nature08699.
19. **Karlas A, Machuy N, Shin Y, Pleissner K-P, Artarini A, Heuer D, Becker D, Khalil H, Ogilvie LA, Hess S, Murer AP, Mller E, Wolff T, Rudel T, Meyer TF.** 2010. Genome-wide RNAi screen identifies human host factors crucial for influenza virus replication. Nature **463:**818–822. http://dx.doi.org/10.1038/nature08760.
20. **Shapira SD, Gat-Viks I, Shum BOV, Dricot A, de Grace MM, Wu L, Gupta PB, Hao T, Silver SJ, Root DE, Hill DE, Regev A, Hacohen N.** 2009. A physical and regulatory map of host-influenza interactions reveals pathways in H1N1 infection. Cell **139:**1255–1267. http://dx.doi.org/10.1016/j.cell.2009.12.018.
21. **Shaw ML, Stone KL, Colangelo CM, Gulcicek EE, Palese P.** 2008. Cellular proteins in influenza virus particles. PLoS Pathog. **4:**e1000085. http://dx.doi.org/10.1371/journal.ppat.1000085.
22. **Arumugaswami V, Remenyi R, Kanagavel V, Sue EY, Ho TN, Liu C, Fontanes V, Dasgupta A, Sun R.** 2008. High-resolution functional profiling of hepatitis C virus genome. PLoS Pathog. **4:**e1000182. http://dx.doi.org/10.1371/journal.ppat.1000182.
23. **Heaton NS, Sachs D, Chen C-J, Hai R, Palese P.** 2013. Genome-wide mutagenesis of influenza virus reveals unique plasticity of the hemagglutinin and NS1 proteins. Proc. Natl. Acad. Sci. U. S. A. **110:**20248–20253. http://dx.doi.org/10.1073/pnas.1320524110.
24. **Beitzel BF, Bakken RR, Smith JM, Schmaljohn CS.** 2010. High-resolution

functional mapping of the Venezuelan equine encephalitis virus genome by insertional mutagenesis and massively parallel sequencing. PLoS Pathog. **6:**e1001146. http://dx.doi.org/10.1371/journal.ppat.1001146.

25. **Wu NC, Young AP, Dandekar S, Wijersuriya H, Al-Mawsawi LQ, Wu T-T, Sun R.** 2013. Systematic identification of h274y compensatory mutations in influenza A virus neuraminidase by high-throughput screening. J. Virol. **87:**1193–1199. http://dx.doi.org/10.1128/JVI.01658-12.
26. **Neumann G, Watanabe T, Ito H, Watanabe S, Goto H, Gao P, Hughes M, Perez DR, Donis R, Hoffmann E, Hobom G, Kawaoka Y.** 1999. Generation of influenza A viruses entirely from cloned cDNAs. Proc. Natl. Acad. Sci. U. S. A. **96:**9345–9350. http://dx.doi.org/10.1073/pnas.96.16.9345.
27. **Hwang S, Kim KS, Flano E, Wu T-T, Tong LM, Park AN, Song MJ, Sanchez DJ, O'Connell RM, Cheng G, Sun R.** 2009. Conserved herpesviral kinase promotes viral persistence by inhibiting the IRF-3-mediated type I interferon response. Cell Host Microbe **5:**166–178. http://dx.doi.org/10.1016/j.chom.2008.12.013.
28. **Li H, Durbin R.** 2009. Fast and accurate short read alignment with Burrows-Wheeler transform. Bioinformatics **25:**1754–1760. http://dx.doi.org/10.1093/bioinformatics/btp324.
29. **Kinde I, Wu J, Papadopoulos N, Kinzler KW, Vogelstein B.** 2011. Detection and quantification of rare mutations with massively parallel sequencing. Proc. Natl. Acad. Sci. U. S. A. **108:**9530–9535. http://dx.doi.org/10.1073/pnas.1105422108.
30. **Nobusawa E, Sato K.** 2006. Comparison of the mutation rates of human influenza A and B viruses. J. Virol. **80:**3675–3678. http://dx.doi.org/10.1128/JVI.80.7.3675-3678.2006.
31. **García-Sastre A, Egorov A, Matassov D, Brandt S, Levy DE, Durbin JE, Palese P, Muster T.** 1998. Influenza A virus lacking the NS1 gene replicates in interferon-deficient systems. Virology **252:**324–330. http://dx.doi.org/10.1006/viro.1998.9508.
32. **Wang W, Riedel K, Lynch P, Chien CY, Montelione GT, Krug RM.** 1999. RNA binding by the novel helical domain of the influenza virus NS1 protein requires its dimer structure and a small number of specific basic amino acids. RNA **5:**195–205. http://dx.doi.org/10.1017/S1355838299981621.
33. **Donelan NR, Basler CF, García-Sastre A.** 2003. A recombinant influenza A virus expressing an RNA-binding-defective NS1 protein induces high levels of beta interferon and is attenuated in mice. J. Virol. **77:**13257–13266. http://dx.doi.org/10.1128/JVI.77.24.13257-13266.2003.
34. **Seo SH, Hoffmann E, Webster RG.** 2002. Lethal H5N1 influenza viruses escape host anti-viral cytokine responses. Nat. Med. **8:**950–954. http://dx.doi.org/10.1038/nm757.
35. **Hayman A, Comely S, Lackenby A, Hartgroves LCS, Goodbourn S, McCauley JW, Barclay WS.** 2007. NS1 proteins of avian influenza A viruses can act as antagonists of the human alpha/beta interferon response. J. Virol. **81:**2318–2327. http://dx.doi.org/10.1128/JVI.01856-06.
36. **Kellogg EH, Leaver-Fay A, Baker D.** 2011. Role of conformational sampling in computing mutation-induced changes in protein structure and stability. Proteins **79:**830–838. http://dx.doi.org/10.1002/prot.22921.
37. **Gack MU, Albrecht RA, Urano T, Inn K-S, Huang I-C, Carnero E, Farzan M, Inoue S, Jung JU, García-Sastre A.** 2009. Influenza A virus NS1 targets the ubiquitin ligase TRIM25 to evade recognition by the host viral RNA sensor RIG-I. Cell Host Microbe **5:**439–449. http://dx.doi.org/10.1016/j.chom.2009.04.006.
38. **Yoneyama M, Kikuchi M, Natsukawa T, Shinobu N, Imaizumi T, Miyagishi M, Taira K, Akira S, Fujita T.** 2004. The RNA helicase RIG-I has an essential function in double-stranded RNA-induced innate antiviral responses. Nat. Immunol. **5:**730–737. http://dx.doi.org/10.1038/ni1087.
39. **Richt JA, García-Sastre A.** 2009. Attenuated influenza virus vaccines with modified NS1 proteins. Curr. Top. Microbiol. Immunol. **333:**177–195. http://dx.doi.org/10.1007/978-3-540-92165-3_9.
40. **Zhou B, Li Y, Speer SD, Subba A, Lin X, Wentworth DE.** 2012. Engineering temperature sensitive live attenuated influenza vaccines from emerging viruses. Vaccine **30:**3691–3702. http://dx.doi.org/10.1016/j.vaccine.2012.03.025.
41. **Whittle JRR, Zhang R, Khurana S, King LR, Manischewitz J, Golding H, Dormitzer PR, Haynes BF, Walter EB, Moody MA, Kepler TB, Liao H-X, Harrison SC.** 2011. Broadly neutralizing human antibody that recognizes the receptor-binding pocket of influenza virus hemagglutinin. Proc. Natl. Acad. Sci. U. S. A. **108:**14216–14221. http://dx.doi.org/10.1073/pnas.1111497108.
42. **Ekiert DC, Wilson IA.** 2012. Broadly neutralizing antibodies against influenza virus and prospects for universal therapies. Curr. Opin. Virol. **2:**134–141. http://dx.doi.org/10.1016/j.coviro.2012.02.005.
43. **Edinger TO, Pohl MO, Stertz S.** 2014. Entry of influenza A virus: host factors and antiviral targets. J. Gen. Virol. **95:**263–277. http://dx.doi.org/10.1099/vir.0.059477-0.
44. **Blight KJ, McKeating JA, Rice CM.** 2002. Highly permissive cell lines for subgenomic and genomic hepatitis C virus RNA replication. J. Virol. **76:**13001–13014. http://dx.doi.org/10.1128/JVI.76.24.13001-13014.2002.
45. **Lohmann V, Körner F, Koch J, Herian U, Theilmann L, Bartenschlager R.** 1999. Replication of subgenomic hepatitis C virus RNAs in a hepatoma cell line. Science **285:**110–113. http://dx.doi.org/10.1126/science.285.5424.110.
46. **Lindenbach BD, Evans MJ, Syder AJ, Wölk B, Tellinghuisen TL, Liu CC, Maruyama T, Hynes RO, Burton DR, McKeating JA, Rice CM.** 2005. Complete replication of hepatitis C virus in cell culture. Science **309:**623–626. http://dx.doi.org/10.1126/science.1114016.
47. **Adachi A, Gendelman HE, Koenig S, Folks T, Willey R, Rabson A, Martin MA.** 1986. Production of acquired immunodeficiency syndrome-associated retrovirus in human and nonhuman cells transfected with an infectious molecular clone. J. Virol. **59:**284–291.
48. **Pleschka S, Jaskunas R, Engelhardt OG, Zrcher T, Palese P, García-Sastre A.** 1996. A plasmid-based reverse genetics system for influenza A virus. J. Virol. **70:**4188–4192.
49. **Pérez-Cidoncha M, Killip MJ, Oliveros JC, Asensio VJ, Fernández Y, Bengoechea JA, Randall RE, Ortín J.** 2014. An unbiased genetic screen reveals the polygenic nature of the influenza virus anti-interferon response. J. Virol. **88:**4632–4646. http://dx.doi.org/10.1128/JVI.00014-14.
50. **Bornholdt ZA, Prasad BV.** 2006. X-ray structure of influenza virus NS1 effector domain. Nat. Struct. Mol. Biol. **13:**559–560. http://dx.doi.org/10.1038/nsmb1099.